Physics and Measurement of Aero-Optical Effects: Past and Present

Eric J. Jumper and Stanislav Gordeyev

Department of Aerospace and Mechanical Engineering, University of Notre Dame, Notre Dame, Indiana 46556; email: jumper.1@nd.edu

Annu. Rev. Fluid Mech. 2017. 49:419–41

First published online as a Review in Advance on August 22, 2016

The *Annual Review of Fluid Mechanics* is online at fluid.annualreviews.org

This article's doi: 10.1146/annurev-fluid-010816-060315

Keywords

aero-optics, wave-front sensors, structure of turbulence, optical character of turbulence

Abstract

The field of aero-optics is devoted to the study of the effects of turbulent flow fields on laser beams projected from airborne laser systems. This article reviews the early and present periods of research in aero-optics. Both periods generated impressive amounts of research activity; however, the types and amount of data differ greatly in accuracy, quality, and type owing to the development of new types of instrumentation available to collect and analyze the aberrated wave fronts of otherwise collimated laser beams projected through turbulent compressible flow fields of the type that form over beam directors. This review traces the activities and developments associated with both periods but particularly focuses on the development of modern high-bandwidth wave-front sensors used in the present research period. We describe how these modern wave-front data are collected and analyzed and the fluid mechanic information that can be gleaned from them; the use of these data in the fundamental study of turbulence is emphasized.

1. INTRODUCTION

The term aero-optics refers to an intersection of the fields of fluid mechanics, optics, optomechanics, and controls; it deals with the aberrations imposed on a large-aperture laser beam propagated through a variable-index turbulent flow field. The study of aero-optics has had two periods of interest or, more to the point, two periods of funding in the United States, both associated with the development of high-speed (transonic) airborne laser systems. The first was in conjunction with the development of the Airborne Laser Laboratory (ALL) in the 1970s and early 1980s, described by Duffner (1997) and Kyrazis (2013). The second, still ongoing, started in conjunction with the development of the AirBorne Laser (ABL) in the early 1990s, described by Lamberson et al. (2005) and Moler & Lamberson (2013). Both the ALL and ABL were US Air Force demonstration developments for high-energy airborne laser systems but made use of very different lasers: ALL used a gas dynamic laser that lased at 10.6 μm, and the ABL used a chemical oxygen iodine laser that lased at 1.314 μm; modern candidates for high-energy airborne laser systems lase at ∼1 μm for weapons systems and ∼1.5 μm for free-space communication systems.

The first period of interest supported a multitude of studies looking at aero-optical environments due to flows that might occur around turrets/beam directors. At the beginning of the period, virtually nothing was known about what turbulence would do to the laser's beam quality, but it was known that optical turbulence in the atmosphere did have deleterious effects on electro-magnetic signals (Tatarski 1961). Optical turbulence is defined as density fluctuations in the air due to atmospheric turbulence and temperature gradients in otherwise constant pressure stratification so that $\rho' \sim T'$. Early theoretical work was built on Tatarski (1961) and four specifically aero-optical efforts, the first by Liepmann (1952), a theoretical treatise looking into aero-optics to determine the effect that the high-speed turbulent boundary layer would have on the sharpness of schlieren systems, and three by Baskins & Hamilton (1952, 1954) and Stine & Winovich (1956), which were experimental studies investigating Liepmann's theory. Beyond these, investigators in the first period had no previous work to guide them and a free hand in determining their directions. There is a comprehensive review of this early work by Jumper & Fitzgerald (2001). For the purpose of this review, we only point out specific milestone developments that continue to influence the efforts in the second period of activity. But we point out a distinction in the second period's understanding of the cause of aero-optical character that directly affects the use of most experimental and computational results obtained in the first period. To do this, we begin with some theoretical presumptions (conventional wisdom) of that first period.

2. EARLY EFFORTS (FIRST INTEREST PERIOD)

2.1. Measurement Approaches and Limitations

In order to study aero-optical effects, one needs to measure the aberrated wave fronts imposed on an otherwise planar wave front for a large-aperture laser projected through aero-optical turbulence. The measurement of the aberrations is a direct result of the air's unsteady density field in the flow given that the air's index of refraction, n, is directly linked to the fluctuating density through the Gladstone-Dale relationship

$$n = 1 + K_{\mathrm{GD}}\rho \tag{1}$$

or using fluctuating quantities

$$n' = K_{\mathrm{GD}}\rho'. \tag{2}$$

From an optical point of view, the variable index of refraction in the shear flow around an airborne beam director can be assumed to be a compact aberrating field. The wave fronts' aberration after passing through the compact aberrating flow is usually quantified by the optical path difference (OPD), although in fact the OPD is the conjugate of the wave fronts' displacement from the mean wave front over the beam's aperture (Klein & Furtak 1986). As has been repeatedly shown, the wave-front aberrations imposed on an otherwise planar wave front propagated through a compact aberrating field, quantified as OPD, are essentially identical to an integration of the index of refraction along paths parallel to the propagation direction and the removal of the mean of these integrated values over the aperture (see Wang et al. 2012). The integration is referred to as the optical path length (OPL):

$$\mathrm{OPL}(x, y, t) = \int_{z_1}^{z_2} n(x, y, z, t)\mathrm{d}z. \tag{3}$$

After removing the spatially averaged component, we find that the OPD is given as

$$\mathrm{OPD}(x, y, t) = \mathrm{OPL}(x, y, t) - \langle \mathrm{OPL}(x, y, t) \rangle. \tag{4}$$

Here the angled brackets denote spatial averaging. Once obtained, $\mathrm{OPD}(x, y, t)$ and the beam intensity profile over the aperture can be used to compute the intensity distribution at the target due only to the aero-optic field using physical optics (Goodman 1996, Born & Wolf 1999); thus, a measurement of $\mathrm{OPD}(x, y, t)$ is clearly imperative to understand how various types of flow fields found around beam directors affect the airborne optical system's performance. At the time of the first period, the only direct $\mathrm{OPD}(x, y, t)$ measurement instruments applied to the aero-optic problem were holography, interferometry, and shadowgraphs (see, e.g., Trolinger 1982). These were capable of measuring the two-dimensional (2D) spatial aberration over the beam aperture at an instant in time [i.e., (x, y, t)]. However, at the frequencies associated with aero-optical aberrations and because framing rates were slow, no temporal information could be measured by these instruments. The methods developed during this period sought only to measure the fluctuating or changing portions of the density field, so double-pulse methods became standard practice in making spatial density measurements. Temporal information was also needed, for which two closely spaced hot wires were used along with two overheat ratios from which theories were developed to extract the fluctuating density (see Rose & Otten 1982). The theory depended on the pressure fluctuations, p', being negligible, i.e., invoking the strong Reynolds analogy (SRA) (Morkovin 1962). As discussed below, the assumption that p' is negligible is clearly in error for some flows.

During this period, Hartmann plates/sensors began to be used to measure wave fronts. Hartmann sensors make use of Huygens' principle that a wave front travels normal to itself. Thus, when a large-aperture laser beam is projected onto and through an opaque plate with a pattern of holes in it, smaller-aperture beams emerge from the holes normal to the wave-front surface, striking the plate at that location. Initially, these slopes were measured by placing a photographic plate at a distance, ℓ, from the perforated plate, with the film first exposed with a pristine beam to form fiducial spot locations and then exposed with a single laser pulse from a laser propagated through the aberrating medium. The slope of the wave front, $\partial W/\partial x$ and $\partial W/\partial y$, is then equal to $\tan^{-1}(\Delta x/\ell)$ and $\tan^{-1}(\Delta y/\ell)$, respectively. These wave-front slopes can then be integrated to reconstruct the wave front. Although not applied to the ALL program, there were some major advances in Hartmann sensors/plates owing to other concomitant Air Force programs trying to image satellites from ground telescopes and subject to atmospheric optical turbulence. Hartmann plates with perforation patterns became lenslet arrays to measure the wave-front slopes over the full aperture and integrate them to obtain a wave-front surface (Hardy 1991, Greenwood &

Primmerman 1993, Horwitz 1993, Schwiegerling & Neal 2014). Another advantage of the lenslet array is that one needs to measure only the displacement of the focused point at the focal plane and know the focal length to measure the average slope of the wave front over the area (clear aperture) of the individual lenslets. This solved two problems. First, it concentrated the incoming, perhaps low-intensity, light onto the focal point and captured essentially all the incoming light (assuming a fill factor of almost 1.0). Second, by providing the average slope over the lenslet by centroiding the spot on the focal plane as the point for obtaining the slope, the lenslet provided a spatial filter dictating how fine a resolution was wanted for the wave front. Also documented by Schwiegerling & Neal (2014) was the replacement of the photographic plates used to record the slope information with electronic devices that included position-sensing devices and charge-coupled device (CCD) arrays, which began in the 1970s and continued through the 1980s.

2.2. Theoretical Constructs

A number of theoretical efforts resulted in formulations for estimating $\mathrm{OPD}_{\mathrm{rms}}$ from other measures of the flow. The most important of these was given by Sutton (1969):

$$\overline{\langle \mathrm{OPD}^2 \rangle} = K_{\mathrm{GD}}^2 \int_0^{z_1} \int_0^{z_1} \mathrm{Cov}_{\rho'}(z, z')\mathrm{d}z'\mathrm{d}z, \tag{5}$$

where K_{GD} is the Gladstone-Dale constant, relating the density and index-of-refraction fluctuations, $n' = K_{\mathrm{GD}}\rho'$, and the overbar defines time averaging. The covariance function is defined as $\mathrm{Cov}'_{\rho}(z, z') = \overline{\{[\rho(z) - \bar{\rho}(z)]\,[\rho(z') - \bar{\rho}(z')]\}}$ (Gladstone & Dale 1863). Because the covariance function requires a two-point measurement, the density covariance function is usually modeled by either an exponential or Gaussian functional form based on a characteristic length scale, Λ, and the square of the fluctuating density, ρ'^2_{rms}, to arrive at a relationship between the $\mathrm{OPD}_{\mathrm{rms}}$ and quantities presumed to be extracted from hot-wire measurements. The resulting Equation 6 is commonly referred to as the linking equation:

$$\overline{\langle \mathrm{OPD}^2 \rangle} = \alpha\ K_{\mathrm{GD}}^2 \int_0^{z_1} \rho^2_{\mathrm{rms}}(z)\Lambda(z)\mathrm{d}z, \tag{6}$$

where the constant α depends on the form of the covariance function equal to 2 if exponential and $\sqrt{\pi}$ if Gaussian (Wolters 1973, Sutton 1985), where Equation 6 is the form derived by Sutton. Jumper & Fitzgerald (2001) showed that the original equation derived using different means by Liepmann (1952) is identical to the linking equation when the Malley supposition (see below) is incorporated into Liepmann's formulation.

The second most important theoretical formulation still used as a measure of performance is the Strehl ratio (SR), which is the on-axis laser intensity at the target (far field), I, divided by the intensity for a perfect (diffraction limited) on-axis intensity, I_{o}, at the target (Mahajan 1982, 1983), the so-called Maréchal approximation:

$$\mathrm{SR}(t) \equiv \frac{I(t)}{I_{\mathrm{o}}} \approx \exp\left\{-\left[\frac{2\pi\ \mathrm{OPD}_{\mathrm{rms}}(t)}{\lambda}\right]^2\right\}. \tag{7}$$

We note that Equation 7 makes use of the $\mathrm{OPD}_{\mathrm{rms}}$ after the tip/tilt has been removed (see below). Steinmetz (1982) showed that Equation 7, which is an instantaneous SR, is also approximately equal to the time average, $\overline{\mathrm{SR}}$, as long as the coherence lengths of the aberrations over the wave front are small compared to the aperture size, A, with the instantaneous $I(t)$ and $\mathrm{OPD}_{\mathrm{rms}}(t)$ replaced with time averages of these quantities. Because this is typically the way Equation 7 is

used, it is usually referred to as the large-aperture approximation. Ross (2009) and Porter et al. (2013a) showed that Equation 7 is actually exact if the aberration spatial statistics are Gaussian.

3. SECOND, MODERN PERIOD

3.1. Measurement Approaches

What has made the modern period of aero-optics research possible is the development of several new, truly high-temporal-bandwidth wave-front sensors (WFS). The first of these was based on an instrument invented by Malley and colleagues (Klein et al. 1990, Malley et al. 1992). This instrument made use of a supposition that the aberrations on the wave front convect due to propagation through a turbulent flow field in which the aberrating structures in the turbulence convect (see **Figure 1**).

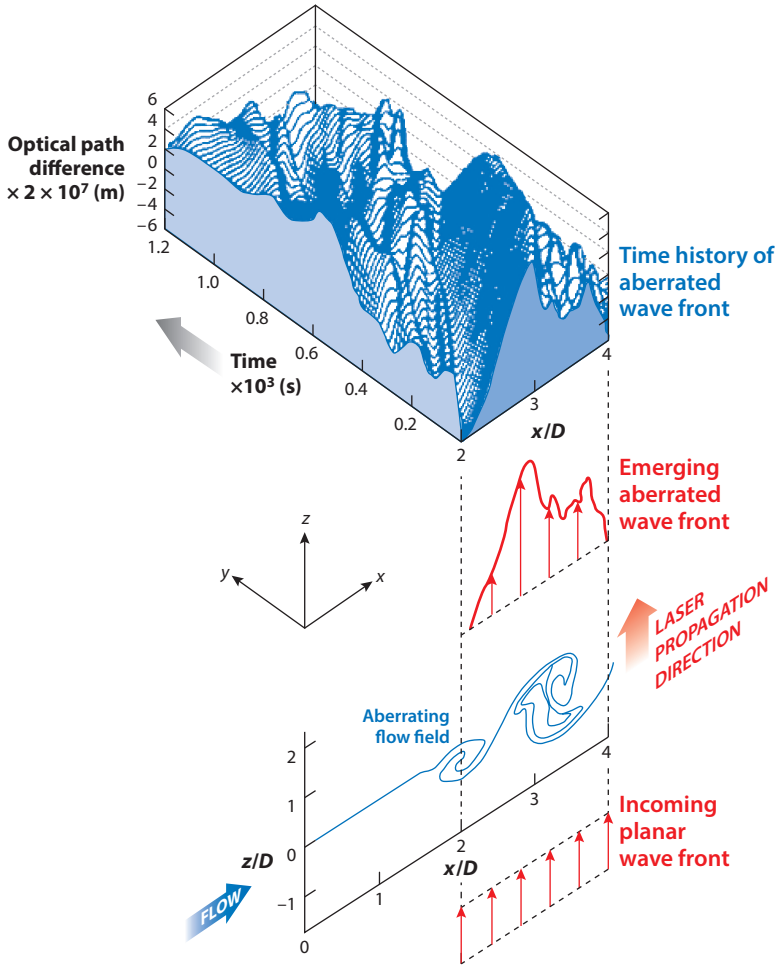

Figure 1

Illustration of the Malley principle. The top of the figure shows 1D wave-front slices in the flow direction as a function of time with high points moving in the flow direction. Figure adapted from Cicchiello & Jumper (1997).

This supposition appears to be self-evident, but in fact it was a breakthrough. It is used so often that the supposition is now referred to as the Malley principle. This principle allowed for the unification of the Liepmann (1952) formulation with that of Sutton (1969) (see Jumper & Fitzgerald 2001). Malley et al. (1992) invented an $\mathrm{OPD}_{\mathrm{rms}}$ measurement device based on this supposition that made use of a single small-aperture laser beam projected through a turbulent flow and measured the time-varying displacement of the beam on a position-sensing device. Based on the underlying principles of the Hartmann sensor, Malley et al. (1992) projected a single small-aperture laser beam through a shear layer and then applied the Reynolds transport theory similar to hot wires to trade time and position. The Malley principle was further developed first by Jumper & Hugo (1995) for large apertures using the small-aperture beam technique (SABT) sensor and then later by Gordeyev et al. (2014b) with a Malley probe. Both made use of multiple small-aperture laser beams so that the wave-front slope and aberration convection speed could be collected at very high bandwidth, with rates up to 1 MHz with the fast digital cameras presently available (Gordeyev & Juliano 2016a,b). In the case of the SABT sensor, the wave fronts extend in the flow direction over a full aperture, whereas with the Malley probe the measurements are made at a single location over an aperture and extended up- and downstream assuming frozen flow and Taylor's hypothesis, $\mathrm{d}x = U_{\mathrm{c}}\,\mathrm{d}t$, where U_{c} is the convection speed. Both the SABT and Malley probe sensors can only reconstruct wave fronts in the flow direction as follows (Gordeyev et al. 2014b):

$$\mathrm{OPL}(x,t) = \int \frac{-\mathrm{d}W(x,t)}{\mathrm{d}x}\mathrm{d}x = -U_{\mathrm{c}} \int \frac{\mathrm{d}W(x,t)}{\mathrm{d}x}\mathrm{d}t. \tag{8}$$

The Malley probe has become ubiquitous for aero-optic characterization and has been extensively used as a nonintrusive turbulent flow instrument, which we address below. The accuracy of the Malley probe in aero-optic characterization was addressed by Hugo & Jumper (1996) using experimental data and by Wang & Wang (2013) using large-eddy simulations.

Another 1D WFS developed in the early 1990s made use of advances in CCD technology. 2D CCD arrays greatly limited the temporal bandwidth at which wave fronts could be collected, and these produced wave fronts only in postprocessing. Position-sensing devices such as lateral effect transducers and quad cells allowed for higher temporal bandwidth and near-real-time wave-front constructions, which were needed for conventional adaptive-optic systems that relied on feedback control (Tyson 1997). By the late 1980s and early 1990s, so-called frame grabbers could be used to capture full CCD arrays so that spot locations under each lenslet forming the subaperture lenslet array could be computationally determined from the CCD data to begin to output wave fronts at much higher than tens of hertz. During the 1990s, real-time WFS were able to output wave fronts up to approximately 1 kHz with a latency of approximately 1 ms. But if the wave fronts were to be postprocessed, image capture rates could be much larger. One such array type that had rates up to 5 kHz was a line-scan camera. Using a line-scan camera, a 1D Hartmann sensor could capture 1D wave fronts regardless of direction. Although this is still much slower than the SABT or Malley probe, the latter two could only reconstruct wave fronts in the flow direction (Neal et al. 1993). One of the first uses of line-scan sensors was in reconstructing full 2D density fields in the plane of the sensors using tomographic reconstruction (McMackin et al. 1997). However, the flow was a heated shear layer rather than a compressible shear layer.

To produce higher-bandwidth, full 2D WFS, investigators developed Hartmann sensors that returned to the use of position-sensing devices. For example, Abado et al. (2010) developed a 10×10 subaperture version that could collect wave fronts at 125 kHz for later processing but could be used for real-time sensing at 100 kHz with only 10^{-5} s of latency. As knowledge of aero-optic aberrations grew to cover most of the relevant flows up to transonic flight speeds, it

was clear that 100 kHz was about four times faster than wave-front collection required. At the same time, CCD technology continued to advance.

By the mid-1990s, very high-bandwidth cameras were being developed and used for fluid mechanics research. Wyckham & Smits (2009) added a lenslet array ahead of the CCD array in a high-bandwidth camera. This marked the first use of the emerging family of high-bandwidth 2D CCD cameras for the measurement of wave fronts. The problem with these early cameras was the limited number of frames that could be stored. However, by the time the position-sensing 10×10 subaperture WFS (Abado et al. 2010) was ready for use, a lenslet array was mounted in front of the CCD array in a Photron FASTCAM-SA1 (Jumper et al. 2013), which allowed for wave-front acquisition at 20 kHz. A later version of a WFS using Phantom cameras made acquisition at 50 kHz routine with very long time series of wave fronts. These types of WFS are now in routine use for aero-optics research.

3.2. Types of Aero-Optical Wave-Front Data Available in the First and Second Periods

In the 1970s, an impressive set of wind-tunnel and flight-test experiments devoted to aero-optical research was performed in support of the ALL program. The NASA Ames 6 ft $\times$ 6 ft tunnel and its 14 ft $\times$ 14 ft tunnel were used in experiments up to Mach 0.9, in flight experiments in a Lear jet and using two KC-135's, and in a single-aircraft experiment on a KC-135. The open literature description of these tests can be found in a collection of papers edited by Gilbert & Otten (1982). The wind-tunnel experiments examined aero-optic time-averaged lensing over a turret (Otten & Gilbert 1982) but with no higher-order wave-front aberrations. The flight experiments used double-pulsed interferometry accompanied by hot-wire measurements but only of the attached turbulent boundary layers. Some separated shear layer experiments were carried out in flight (Rose et al. 1982). However, these were not optical experiments but instead used hot wires. As mentioned above, the hot-wire measurements were connected to the $\mathrm{OPD}_{\mathrm{rms}}$ through Equation 6, but obtained ρ' from the hot-wire data, using Morkovin's SRA, which assumed p' was negligible.

In the second (present) period, not only has the instrumentation vastly improved, but the facilities are now more extensive. For example, aero-optical testing has now been performed at subsonic speeds at the Arnold Engineering and Development Center (AEDC; Hugo et al. 1997, Fitzgerald & Jumper 2002) and in the SARL and TGF wind tunnels at the Wright-Patterson Air Force Base (Vukasinovic et al. 2008, 2011; Ponder et al. 2011; Smith et al. 2014a; Wittich et al. 2014). Testing has also been performed at sub-, trans-, and supersonic speeds at the Air Force Academy (Gordeyev et al. 2007a,b, 2012, 2014b, 2015b; Siegel et al. 2009; Nguyen et al. 2015); at sub-, trans-, and supersonic speeds at the University of Notre Dame (Rennie et al. 2008; Ponder et al. 2010; Porter et al. 2013b,c; Ponder & Jumper 2011; Gordeyev et al. 2014b, 2015a; Houpt et al. 2016); and at hypersonic speeds at Purdue University (Gordeyev & Juliano 2016a,b). Moreover, tests have been conducted at the California Institute of Technology (Saxton-Fox et al. 2014, 2015; Gordeyev et al. 2015c), Auburn University (Reid et al. 2010, 2013), University of California, Irvine (Zubair & Catrakis 2007), and other locations. Additionally, two flight programs, the Airborne Aero-Optics Laboratory (Jumper et al. 2013) and the Airborne Aero-Optics Laboratory–Transonic (Jumper et al. 2015), have been routinely used for in-flight aero-optics experiments. These flight experiments were used to collect ubiquitous wave-front data for a variety of turret configurations, as well as to flight test flow-control methods, developed from theory and wind-tunnel studies. These data have formed the basis for a large number of studies of aero-optic and adaptive-optic studies (see, e.g., Jumper 2013).

4. EVOLVING UNDERSTANDING OF AERO-OPTICS

4.1. Free Shear Layers

The first use of the new high-bandwidth WFS was the SABT sensor to interrogate a Mach 0.8 shear layer at the AEDC (Hugo et al. 1997, Fitzgerald & Jumper 2002). As noted by Fitzgerald & Jumper (2002), the AEDC facility was designed and constructed under the assumption that the Rose (1979) supposition that p' was negligible, and hot-wire measurements made in wind tunnels for a shear layer suggested that turbulence coherence lengths were quite small. As such, the AEDC interrogation windows were only 5 cm in diameter. These windows represented a spatial filter (Hugo et al. 1997) that could be incorporated into the wave-front reconstructions by appropriately filtering the slope data in time. After the application of the temporal/spatial filter, the OPD_{rms} at the station 2 window, centered at 48.3 cm from the shear layer splitter plate, ranged from 0.0639 μm to 0.165 μm, which at the time was considered large based on data derived from hot wires in the 1970s and 1980s. By adjusting the temporal/spatial filter so that only vibration was removed, Fitzgerald & Jumper (2002) showed that the OPD_{rms} was really approximately 0.3 μm. Even with the temporal/spatial filter adjusted, as indicated in Equation 4, the mean for each frame was still removed over the 5-cm aperture. Fitzgerald & Jumper (2002) showed that reconstructing the true wave front over a more extended aperture yielded a coherence length of the turbulence of approximately 11.3 cm, which would again increase the OPD_{rms}. When these data were first reported at a national meeting (Fitzgerald & Jumper 2000), they caused extensive discussion and disbelief based on the theory of the cause of the aberrations that grew out of work in the 1970s, 1980s, and 1990s. This prompted revisiting the theory; in the end, for separated shear layers, it was shown that the SRA presuming that p' was negligible was completely incorrect. Coherent vortical structures form in separated shear layers due to the Kelvin-Helmholtz instability, and these structures are concomitant with deep pressure wells so that p' is extremely large and cannot be neglected (Fitzgerald & Jumper 2004). In fact, the low-pressure wells, with their concomitant low density, dominate the cause of the aberrations seen in the separated shear layer.

It seems almost incomprehensible now, but in the mid-1990s the computation of high-speed compressible shear layers lay at the fringes of what could be computed (Wang et al. 2012). As such, it was determined that the pressure wells were the dominating cause of shear layer aberrations by overlaying a shear layer's velocity field with a thermodynamic model to extract the pressure, temperature, and density using a method often referred to as the weakly compressible model, which has been shown repeatedly to closely predict the experimentally observed aberration field (Fitzgerald & Jumper 2004; Nightingale et al. 2009, 2013; Ponder et al. 2010). More recently, large-eddy simulations of free shear layers have shown that, in free shear layers, the dominant influence on density fluctuations results from the unsteady pressure associated with the coherent structures that form in a free shear layer (Seidel et al. 2009, Visbal 2009, Wang & Wang 2009).

The fact that p' is primarily responsible for the aberrating structures in a free shear layer has several important ramifications. The first has to do with measurements of OPD_{rms} for free shear layers made using hot wires, as discussed in Section 2. Given that the method of extracting ρ' depended on the assumption that p' was negligible, these measurements grossly underestimated the real OPD_{rms}. Because the application of these measurements was for the ALL, which used a gas dynamic laser that lased at 10.6 μm, this underestimate had little consequence. However, these gross underestimates of the true impact of the measurements significantly impacted airborne laser systems that would use much shorter wavelength lasers, such as the chemical oxygen iodine laser in the ABL (Gilbert 1982, Jumper et al. 2013). **Figure 2** shows the effect on the on-axis intensity of a diffraction-limited beam in the far field ratioed by that for a laser wavelength, λ, of

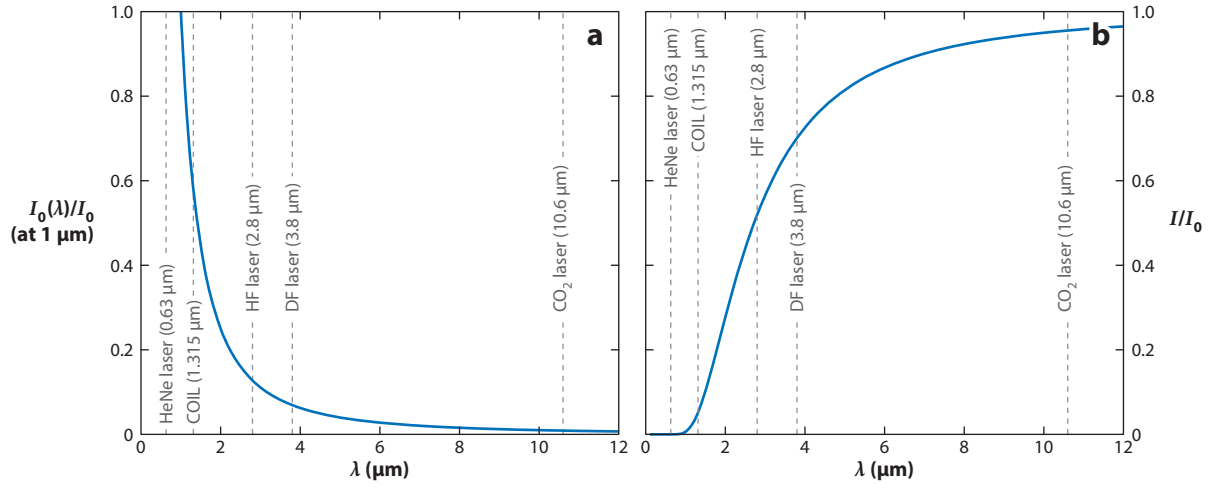

Figure 2

(*a*) The diffraction-limited, on-axis intensity for a given aperture size and range of a laser as a function of wavelength, λ, divided by that at 1 μm. (*b*) Ratio of actual on-axis intensity to diffraction-limited intensity due to OPD_{rms} level that would produce a 95% ratio at 10.6 μm. Figures adapted from Jumper et al. (2013). Abbreviations: COIL, chemical oxygen iodine laser; DF, deuterium fluoride laser; HF, hydrogen fluoride laser; OPD, optical path difference.

1.0 μm. The curve in **Figure 2*b*** uses Equation 7 to estimate the reduction in the SR for the same aero-optic wave-front aberration that would lead to only a 5% reduction for the ALL wavelength as a function of laser wavelength, λ.

The assumption that p' was negligible also affected computational predictions of the aberrating effect of free shear layers. Computational methods that made use of Reynolds-averaged Navier-Stokes (RANS) and even unsteady RANS methods in which the turbulence models suppressed the formation of coherent structures in free shear layers gave rise to gross underpredictions. These methods extracted the values of the velocity fluctuations associated with the turbulence models being used and then estimated the density fluctuations employing the same models used with the hot-wire measurements used to predict ρ'. Examples of this mistaken approach can be found in Pond & Sutton (2006) and Cassady et al. (1989), for example.

The availability of high-bandwidth WFS and the understanding of the cause of the aberrations in a free shear layer have allowed for ubiquitous experimental data from both wind tunnels and flight experiments. As discussed by Gordeyev & Jumper (2010), these data can be divided into that for fully subsonic flow over the beam director, that for incoming flow above the critical Mach number so that the flow becomes supersonic over part of the beam director (i.e., transonic), and that for the case in which the incoming flow is supersonic. Although some data, both experimental and computational, do exist for incoming supersonic flow (Gao et al. 2012a,b), for the purpose of this review we consider only fully subsonic flow and some extension into transonic flow characteristics of the separated shear layer. The aero-optical environment is very similar for both sub- and transonic flow when propagating through the separated flow in the wake of the turret. However, in transonic flow, a shock forms over the beam director and causes the flow to separate at different and temporally changing locations, so this adds to the already unsteady aberrating field caused by the separated wake but does not significantly modify the basic character of the aero-optical environment for propagating in the aft direction (Morrida et al. 2016a,b). In fact, propagation

through at least a portion of the separated flow on a beam director is much like the experiments for propagation through a separated shear layer created by incoming parallel streams of air. In fact, the compressible shear layer facility at the AEDC, mentioned above, first alerted the community to the magnitude of the aero-optic problem when propagating through separated flows off of beam directors. The use of data from the AEDC experiments (Hugo et al. 1997), data from a similar facility at Notre Dame, and even data obtained from a low-speed heated jet (McMackin et al. 1995) began to connect the character of the wave-front aberrations with the flow physics (Fitzgerald & Jumper 2004).

In their investigation of the underlying flow physics, Fitzgerald & Jumper (2004) used the magnitude and spatial/temporal character of the aberrated wave fronts to examine what must be going on in the compressible shear layer to explain the spatial and temporal character of the wave fronts collected at the AEDC (see discussion above). As obvious as this now seems, the supposition of large pressure fluctuations in separated shear layers was really a revolutionary idea because at the time pressure fluctuations in a separated shear layer were presumed to be negligible by the SRA, mentioned above as causing the fatal flaw in the use of hot wires to infer density fluctuations. But more subtle characteristics of the turbulent flow were able to be extracted from information contained in the wave fronts and even in the raw slope data used to construct them.

Liepmann's (1952) analysis mentioned in Section 1 actually derived the jitter (mean-square deflection angle) of a single small-diameter light beam passing through a high-speed turbulent boundary layer using geometric optics. Let us recall that this is actually the time-varying slope of a larger beam that had this point in its aperture. After propagation through a boundary layer of thickness δ, in the propagation direction, y, Liepmann's analysis gave

$$\langle\theta^2\rangle = \frac{1}{[n_o(\delta)]^2}\int_0^\delta\int_0^\delta n_o(y)n_o(\zeta)\left\langle\left(\frac{\partial\upsilon}{\partial y}\right)^2\right\rangle R_\upsilon(|y-\zeta|)\mathrm{d}y\,\mathrm{d}\zeta, \tag{9}$$

where the index of refraction is $n = n_o(y)(1+\upsilon)$, and $R(|y-\zeta|)$ is the correlation function for the index variation. When the index-of-refraction fluctuation, υ, is replaced by the density fluctuation, ρ', $\upsilon = (\rho' K_{GD})/n_o$, Equation 9 becomes

$$\langle\theta^2\rangle = \left[\frac{K_{GD}}{n_o(\delta)}\right]^2\int_0^\delta\int_0^\delta\left\langle\left(\frac{\partial\rho'}{\partial y}\right)^2\right\rangle R_{\rho'}(|y-\zeta|)\mathrm{d}y\,\mathrm{d}\zeta. \tag{10}$$

As pointed out by Jumper & Fitzgerald (2001), the same jitter used to construct the wave fronts from a Malley probe actually contains important information about the fluid mechanics. Although it was developed for the passage of a small beam through a turbulent boundary layer, Hugo & Jumper (1996) demonstrated that Equation 10 also applies to shear layers. Thus, as was suggested by Liepmann, Equation 10 has always held the promise of being able to use the jitter data as a nonintrusive flow diagnostic tool (Hugo & Jumper 2000). The errors made in the earlier period of aero-optics in using Equations 5, 6, and 10 were not in their formulation but rather in the assumption of the SRA in measuring the fluctuation density and its correlation length using hot wires.

In the mid-1990s, 1D wave fronts were also used to investigate basic fluid mechanic processes in shear layers. In addition to the use of the line-scan version of the wave fronts to construct 2D density fields using tomographic reconstruction (McMackin et al. 1997), line-scan wave fronts were also used to visualize coherent vortex convection velocities and paring events in a forced free shear layer for heated jets (McMackin et al. 1995).

Siegenthaler & Jumper (2007) employed a Malley probe to develop an aperture function that demonstrated the effectiveness of a tip/tilt mirror, usually referred to as a fast steering mirror, to

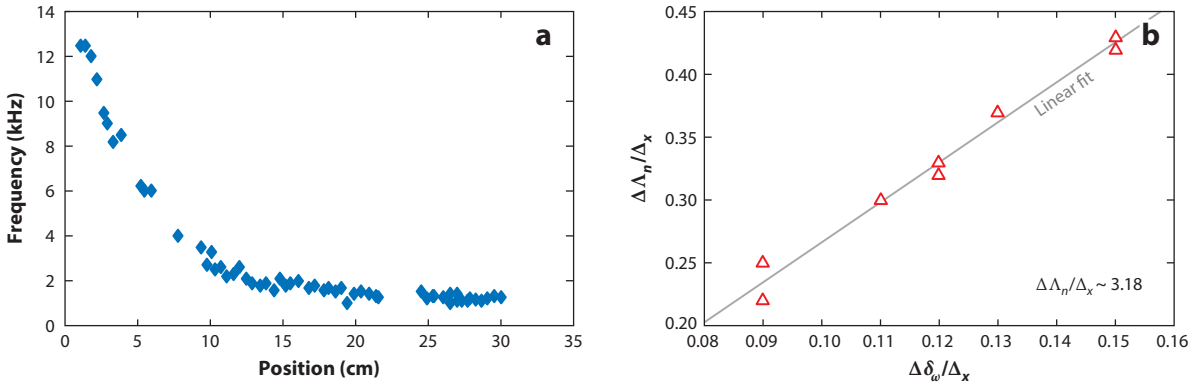

Figure 3

(*a*) Peak in small-aperture beam deflection angle spectra versus position downstream from the splitter plate for a compressible shear layer. Panel *a* adapted from Siegenthaler et al. (2005). (*b*) Optical coherence length versus shear layer vorticity thickness. Panel *b* adapted from Nightingale et al. (2009) with permission of the American Institute of Aeronautics and Astronautics.

reduce the wave-front error, making use of a compressible shear layer. They showed that studying the spectrum of a single small-aperture beam directed through the shear layer could capture the character of the shear layer, which had been studied for decades with hot-wire methods. The aperture function analysis would have been useful in initially interpreting the AEDC data, but Fitzgerald & Jumper (2002) in effect made use of the underlying principles to recreate the aberrations seen in the 5-cm window leading to the supposition that the underlying length scale of the large structures passing by the window was approximately 11.5 cm in length. These principles are useful in extrapolating data taken over a small area to much larger distances up- and downstream.

Nightingale et al. (2009) made further use of the spectra of a single small-aperture beam directed through a shear layer to extract the layer's characteristics, studying the character of forced and unforced compressible shear layers. **Figure 3** shows the relationships found by Siegenthaler et al. (2005) and Nightingale et al. (2009) between the beam deflection angles and the shear layer coherent vortex size, as well as the growth of the shear layer, demonstrating the use of a single beam in performing nonintrusive measurements for fluid mechanics. The single-beam approach was later used in a feedback loop to control an adaptive optic system for the forced shear layer (Nightingale et al. 2013). With the small-beam technique, Smith et al. (2011) demonstrated that analyzing the beam time series can provide information about the structure sizes, typical frequencies, and convective speeds. These examples, as well as more examples in the next section, demonstrate that aero-optical effects can be used to nonintrusively measure the flow characteristics.

Unlike the situation at the time of the first temporally resolved wave-front measurements made at the AEDC, compressible methods for computing separated shear layers have now become routine, and to first order, the predicted wave fronts simulating laser propagation normal to a shear layer appeared to come close to predicting the experimentally observed OPD_{rms} (Visbal 2009, Wang & Wang 2009). Yet when wave fronts (Ponder & Jumper 2011), schlieren (Weston & Jumper 2002, Wittich 2009), and laser-induced fluorescence (Reid et al. 2013) were used to examine laser propagation along the span of total-temperature-matched compressible shear layers, there were distinct differences in predicted and measured density fields. These differences present a conundrum that has yet to be resolved.

4.2. Attached Turbulent Boundary Layers

As mentioned in Section 1, attached turbulent boundary layers were the first aero-optic flows studied to quantify the crispness of schlieren photographs (Liepmann 1952, Stine & Winovich 1956) or interferograms (Small & Weihs 1976) and led to the development of Equations 5, 6, and 10. Unlike shear layers, in which the pressure fluctuations were found to be the dominant cause of the aero-optical distortions, numerous experimental (Spina et al. 1994, Smits & Dussauge 1996) and numerical (Gaviglio 1987, Guarini et al. 2000, Duan et al. 2010, Wang & Wang 2013) studies in boundary layers have shown that the time-averaged pressure fluctuations are several times smaller than temperature fluctuations. Consequently, the SRA, in which the main assumption is to neglect the pressure fluctuations, is commonly used in the study of boundary layers (Spina et al. 1994). To be more precise, the SRA states that the temperature (and hence the density) fluctuations are only related to the local velocity fluctuations via adiabatic cooling/heating:

$$\frac{\rho_{\mathrm{rms}}(y)}{\bar{\rho}(y)} = \frac{T_{\mathrm{rms}}(y)}{\bar{T}(y)} = A(y)(\gamma-1)\frac{\bar{U}(y)u_{\mathrm{rms}}(y)}{a^2(y)}, \tag{11}$$

where a is the local speed of sound, and an overbar denotes the local mean quantities. The function $A(y)$ in Equation 11 takes into account the stress integral distribution in the boundary layers and was found to be approximately unity inside boundary layers (Smith & Smits 1993, Smits & Dussauge 1996, Guarini et al. 2000, Duan et al. 2010).

One of the first specifically aero-optic experimental studies of distortions caused by turbulent boundary layers made use of hot wires to measure velocity fluctuations to infer density fluctuations using the SRA (Rose 1979). Direct double-pulse interferometry measurements for propagation through attached turbulent boundary layers were performed by Gilbert (1982). Masson et al. (1994) compared Rose's estimations using hot wires with Gilbert's and found, after removing a systematic error, that the two generally agreed.

These early measurements, owing primarily to a lack of necessary accuracy, had conflicting conclusions about the $\mathrm{OPD}_{\mathrm{rms}}$ dependence on the boundary layer parameters. Rose (1979) suggested that $\mathrm{OPD}_{\mathrm{rms}} \sim q\delta$, where q is the dynamic pressure and δ is the boundary layer thickness, whereas Gilbert (1982) concluded that $\mathrm{OPD}_{\mathrm{rms}} \sim q^{1/2}$. Masson et al. (1994) proposed that $\mathrm{OPD}_{\mathrm{rms}} \sim (\rho_\infty M^2)^{1.16}$. The last two dependences contradict the general, similarity-based scaling derived by Gordeyev & Jumper (2010), who showed that $\mathrm{OPD}_{\mathrm{rms}}$ is proportional to the free-stream density and the boundary layer thickness, $\sim \rho_\infty \delta f(M, Re)$.

With the development of the Malley probe in the 1990s, one of the first temporally resolved (>100 kHz) optical measurements for subsonic turbulent boundary layers (Gordeyev et al. 2003, Wittich et al. 2007) showed that aero-optical distortions scaled as $\mathrm{OPD}_{\mathrm{rms}} \sim \delta\rho M^2$. Additionally, the spectra for the wave-front slope (i.e., small-aperture beam jitter) showed that the dominant deflection-angle frequencies were on the order of U_∞/δ and convection speeds for the aero-optical aberrations convected at a speed of 0.82–$0.85U_\infty$. All these findings, complemented by recent high-fidelity numerical studies of aero-optical effects in turbulent boundary layers (White & Visbal 2012, 2013; Wang & Wang 2013; Kamel et al. 2016), suggested that the optically active structures reside in the outer portion of the boundary layer. Wyckham & Smits (2009) pioneered the use of a high-speed digital camera for Shack-Hartmann wave-front sensing to measure aero-optical distortions in both subsonic and supersonic boundary layers. They used a bulk-flow approach to derive the OPD dependence:

$$\mathrm{OPD}_{\mathrm{rms}} = C_w K_{\mathrm{GD}} \rho_\infty \delta M^2 \sqrt{C_f}\, r_2^{-3/2}, \tag{12}$$

where $r_2 = 1 + \frac{\gamma-1}{2}M^2[1 - r(U_c/U_\infty)^2]$ for adiabatic walls; from their experiments, the C_w constant was estimated to be 0.6. Gordeyev et al. (2014b, 2015a) used the SRA in the form of

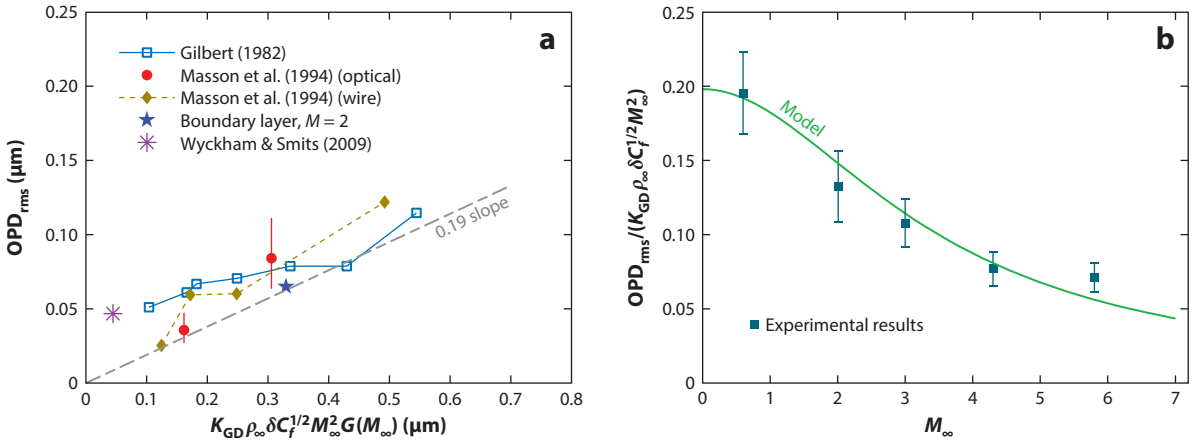

Figure 4

(*a*) Some of early $\mathrm{OPD_{rms}}$ measurements in subsonic boundary layers, plotted versus the dependence given in Equation 13. Panel *a* adapted from Gordeyev et al. (2014b). (*b*) A comparison of the normalized $\mathrm{OPD_{rms}}$ scaling (Equation 13) with experimental data for supersonic and low-hypersonic Mach numbers. Panel *b* adapted from Gordeyev & Juliano (2016a). Abbreviation: OPD, optical path difference.

Equation 11 and the linking equation (Equation 6) and derived a similar functional dependence for $\mathrm{OPD_{rms}}$:

$$\mathrm{OPD_{rms}} = BK_{\mathrm{GD}}\rho_\infty \delta M_\infty^2 \sqrt{C_f} F(M_\infty). \tag{13}$$

Using commonly accepted velocity profiles, Gordeyev et al. found the constant B to be 0.2. Both functional forms, with an adjusted $C_w = 0.2$ and the added U_c dependence with Mach number (discussed below) for Equation 12, were found to give very similar predictions up to $M = 6$ (Gordeyev et al. 2015b, Gordeyev & Juliano 2016a). **Figure 4*a*** shows some of the early aero-optical measurements, mentioned above and rescaled using Equation 13. The data generally agree well with the functional dependence, with larger deviations at low $\rho\delta$ values, where values of $\mathrm{OPD_{rms}}$ are small. These deviations primarily result from a lack of accurate optical measurements for these low $\mathrm{OPD_{rms}}$ values.

A comparison of experimental measurements in supersonic flow (Gordeyev et al. 2012, 2015b) and low-hypersonic flow (Gordeyev & Juliano 2016a) shows that the scaling (Equation 13) correctly predicts aero-optical distortions up to Mach 5 (**Figure 4*b***). Although there is a small deviation at Mach 5.8, a deviation at some Mach number above 3–5 should be anticipated because some of the assumptions used to develop Equation 13 are not expected to remain valid beyond Mach 3–5 (Gordeyev et al. 2015a, Gordeyev & Juliano 2016a). In fact, it is somewhat surprising that Equation 13 performs as well as it does up to and even beyond Mach 5.

Moreover, Gordeyev et al. (2015b) and Gordeyev & Juliano (2016a) showed that the deflection-angle spectra, measured by a small-aperture beam, peaked at approximately $St_\delta = 0.9$ over a wide range of Mach numbers, up to Mach 6. That St_δ has a maximum of approximately 0.9 over a range of Mach numbers from low subsonic (Smith et al. 2014b) to 6 shows that the use of a single small-aperture laser beam through the boundary layer and measurement of its deflection-angle dynamics is a useful nonintrusive means of measuring boundary layer thickness over a wide range of Mach numbers (Nguyen et al. 2015).

Experimentally measured convective speeds, related to aero-optical distortions (Gordeyev et al. 2012, 2015b; Gordeyev & Juliano 2016a), demonstrated that the speed monotonically increases

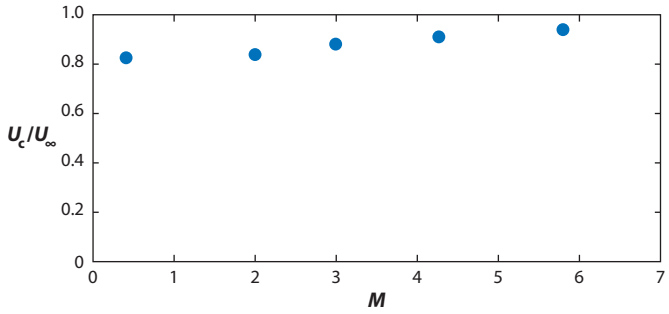

Figure 5

Experimentally measured normalized convective speeds of aero-optical structures. Figure adapted from Gordeyev & Juliano (2016a).

with Mach number, from $0.82U_\infty$ at subsonic speeds to $0.95U_\infty$ at Mach 5.8 (**Figure 5**). These convective speeds are similar to convective-speed measurements reported by Speaker & Ailman (1966) and Spina et al. (1991). Numerical simulations by Maeder et al. (2001) for $M = 0.9$ and 2.3, and Tromeur et al. (2003) for $M = 3$, 4.5, and 6, showed that the density fluctuations for supersonic speeds are suppressed near the wall owing to higher flow temperatures there. At supersonic speeds, optically active structures away from the wall became relatively stronger, resulting in higher observed aero-optical convective speeds.

As mentioned above, the SRA has been shown to be approximately valid for adiabatic turbulent boundary layers for predicting $\mathrm{OPD}_{\mathrm{rms}}$ values (Gordeyev et al. 2014b). It has also been shown to predict $\mathrm{OPD}_{\mathrm{rms}}$ for nonadiabatic wall boundary layers (Gordeyev et al. 2015a). The nonadiabatic wall predictions of $\mathrm{OPD}_{\mathrm{rms}}$ that gave a dependence on wall-temperature mismatch, $\Delta T = T_{\mathrm{w}} - T_{\mathrm{r}}$ (with T_{w} the wall temperature and T_{r} the recovery temperature), have been experimentally observed by Cress et al. (2010). In addition to being able to reduce $\mathrm{OPD}_{\mathrm{rms}}$ by cooling the wall, an important consequence of the ΔT dependence is that introducing a positive temperature mismatch makes it possible to thermally label and measure 3D large-scale structures using WFS in incompressible boundary layers (Smith et al. 2014b, Gordeyev et al. 2015c, Smith 2015). Moderately heating the wall also makes it possible to measure optical aberrations and therefore extract fluid mechanic information for an incompressible turbulent boundary layer (Saxton-Fox et al. 2014, 2015; Gordeyev et al. 2015c).

When applied to the description of aero-optical distortions for moderately cooled walls, the model (Equation 13), modified to include wall temperature effects given by (Gordeyev et al. 2015a)

$$\mathrm{OPD}_{\mathrm{rms}} = B \cdot K_{GD}\rho_\infty \delta \sqrt{C_f}\left[M_\infty^4 + C_1 \frac{\Delta T}{T_\infty} M_\infty^2 + C_2\left(\frac{\Delta T}{T_\infty}\right)^2\right]^{1/2}, \qquad (14)$$

provided a functional dependence form, which agreed with experiments (Gordeyev et al. 2015a) and numerical simulations (White & Visbal 2013), but it overestimated the reduction of $\mathrm{OPD}_{\mathrm{rms}}$ near $\Delta T/(T_\infty M_\infty^2) = -0.4$ (see **Figure 6*a***). Additionally, it improperly predicted the convective speeds for moderately cooled walls (**Figure 6*b***). Yet when the pressure is allowed to vary inside the boundary layer, a better prediction of both the $\mathrm{OPD}_{\mathrm{rms}}$ levels and convective speeds can be made (see **Figure 6**). Gordeyev et al. (2015a) showed that in moderately cooled boundary layers, temperature fluctuations are suppressed owing to the total temperature variation in the wall-normal direction, whereas the pressure fluctuations are not significantly modified.

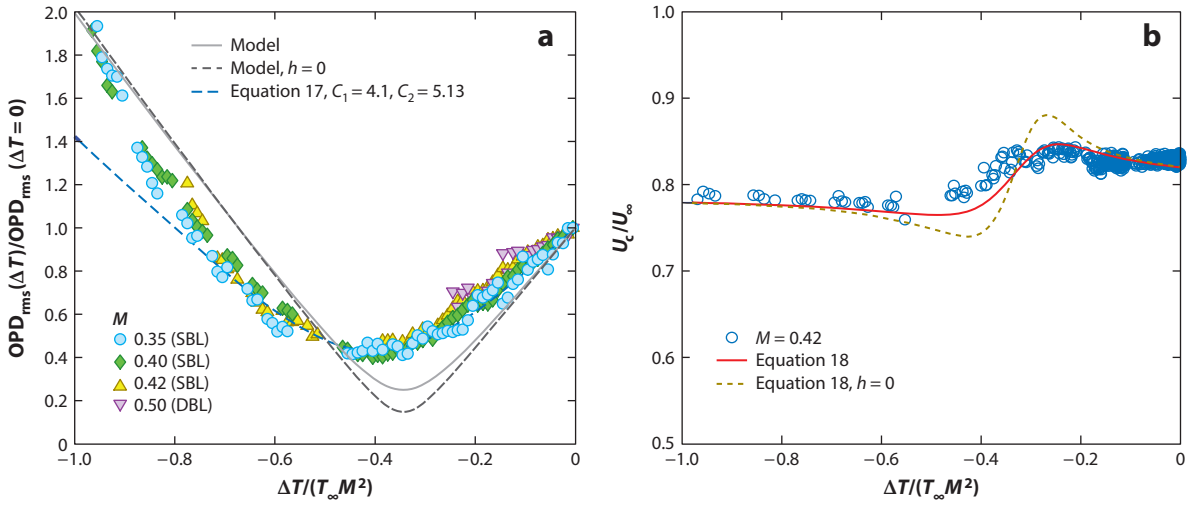

Figure 6

(*a*) OPD_{rms} normalized by the adiabatic wall OPD_{rms} value versus $\Delta T/(T_\infty M_\infty^2)$, the best-fit and the model predictions with and without ($h = 0$) the pressure term. (*b*) Convective speed of aero-optical structure as a function of the wall temperature and the model prediction with and without the pressure term. Equations 17 and 18 are provided in Gordeyev et al. (2015a). Figure adapted from Gordeyev et al. (2015a) with the permission of AIP Publishing. Abbreviations: DBL, double boundary layer; OPD, optical path difference; SBL, single boundary layer.

To further study the effect of pressure fluctuations, Gordeyev et al. (2015c) and Gordeyev & Smith (2016) simultaneously measured the velocity field and overall wave fronts in a subsonic boundary layer. With the requirement that the pressure fluctuations are zero, the density field and resulting wave fronts can be computed from the velocity field, using an instantaneous version of the SRA. Instances in which the pressure fluctuations cannot be ignored were identified and studied by comparing the computed wave fronts using the velocity field via the SRA approach to the measured wave fronts. An identified instance, in which pressure fluctuations appear, was found to correlate with the presence of large-scale vortical structures. As discussed above, the pressure fluctuations inside shear layers with vortical structures significantly contribute to the overall aero-optical distortions (Gordeyev & Smith 2016). Therefore, these simultaneous velocity/wave-front studies, as well as recent studies in adverse-pressure boundary layers (Thomas 2015; F.O. Thomas & D.M. Schatzman, manuscript under review), provide growing evidence that local shear layer–type structures with associated lower-pressure regions may play an important role in the boundary layer dynamics.

Ranade et al. (2016) studied the effect of large-scale free-stream pressure fluctuations imposed on turbulent boundary layers and found that the pressure fluctuation-induced velocity fluctuations in the boundary layer modulated the amplitude of the boundary layer small-scale structures. The study was instigated by wave-front anomalies observed when measuring wave fronts for a large-aperture laser beam projected through a forced shear layer but also capturing the turbulence in the compressible boundary layer over the high-speed optical window (Duffin 2009). Finally, recently high-speed WFS were successfully used to study the topology and dynamics of various transitional features, turbulent bursts and modal waves, in laminar hypersonic boundary layers (Gordeyev & Juliano 2016b).

5. WAVE-FRONT DATA AND THEIR USES

In the case of geometrically simple fundamental flows, such as turbulent shear and boundary layers, aero-optical spatially temporally evolving wave fronts depend only on the aperture size and flow parameters such as the local thickness and convective speed. In the case of the flow around application-important geometries, such as turrets, the flow is fairly complex and consists of the attached boundary layer in the front portion of the turret, the initial separation region with the shear layer–dominant structures, and a highly 3D wake downstream of the turret (Gordeyev & Jumper 2010). Only some of these data are available in the open literature, and they take the form of wave-front data over cylindrical turrets (Gordeyev et al. 2011, 2013; Vorobiev et al. 2014), cylindrical turrets with flow control (Gordeyev et al. 2005, 2013; Wang et al. 2010), hemispherical turrets with flat windows (De Lucca et al. 2013), hemispherical turrets with conformal windows (Vukasinovic et al. 2008, De Lucca et al. 2013, Morrida et al. 2016b), and hemispherical turrets on a cylindrical base with flat and conformal windows (Gordeyev at al. 2007a,b; Vukasinovic et al. 2011; Porter et al. 2013b; Morrida et al. 2016a). All these cases report wave-front data for fully subsonic and transonic flow over the turrets. For these complex geometries, the distorted wave fronts, in addition to being functions of the 2D aperture and time, depend on other parameters, such as the viewing angle of the direction of the beam with respect to the turret or the beam director's field-of-regard angle, the turret's geometry, and the flow regime.

Historically, time-averaged levels of OPD_{rms} were reported as a function of flow and turret parameters due to the low wave-front sampling rates. OPD_{rms} is enough to estimate the far-field intensity, using Equation 7. However, with the development of high-bandwidth WFS and various experimental and numerical studies of aero-optical environments around different turrets, the question of how to analyze, rescale, and compare these optical data arose.

As mentioned above, the analysis of the wave fronts, or more specifically their deflection-angle spectra, provides a new nonintrusive fluid mechanic instrument. But to extract meaningful information from the wave front over the full aperture for aero-optic disturbances, one must reduce the wave fronts into meaningful modes. Traditionally, wave fronts have been decomposed using Zernike polynomials (Noll 1976), which are useful in identifying aberrations due to tip tilt, defocus, coma, etc. Although these are useful characteristics, they have come into existence for the analysis of cylindrical optical systems. As discussed above, aero-optical disturbances result from fluid mechanic disturbances that convect and tend to align themselves with a direction related to the flow. These same characteristics are imposed on the wave front of a beam projected through them. An important step acknowledging the fundamentally non-Zernike nature of aero-optic wave fronts was the application of proper orthogonal decomposition (POD; Berkooz et al. 1993) to the decomposition of aero-optic wave fronts (Cicchiello & Jumper 2001). POD is identical to the Karhunen-Loève decomposition in optics. The use of POD has been shown to optimally decompose the spatiotemporal wave fronts into their spatial modes ordered by the most to least aberrating modes and their corresponding temporal eigenvalues. The most aberrating portions of the wave fronts can then be reconstructed as a sum of the first few modes. Since the demonstration of the utility of POD, a closely related decomposition, dynamic mode decomposition (Schmid 2010), has also been shown to be useful (Goorskey et al. 2013a,b). Starting with work by Cicchiello & Jumper (2001), wave-front POD/dynamic mode decomposition began to show up in papers analyzing the temporal-spatial properties of the wave fronts (Seidel et al. 2009; Gao et al. 2012b; Goorskey et al. 2013a,b; De Lucca et al. 2014; Mathews et al. 2016).

When POD is applied to different data sets, it produces spatial modes that are different for different sets (see, e.g., Goorskey et al. 2013a,b), making direct comparison difficult. Recently, a novel way to compare data sets for different geometry conditions was proposed by Gordeyev

et al. (2014a), termed joint POD. Joint POD makes use of data from all the cases being studied and computes modes that are common for all sets. By comparing the amplitudes and spectra of the eigenvalues between cases for the same modes, similarities and differences between data sets become instructive. Although the method was demonstrated on spatiotemporal surface pressure fields, it is now being applied to the comparison of wave-front dynamics between different conditions.

POD provides the fastest convergent set of spatial modes and naturally gives a low-order representation of wave-front data sets. Because of these properties, widespread usage of POD of wave-front data is being applied to the analysis of adaptive-optic corrections (Faghihi et al. 2013; Whiteley et al. 2013; Burns et al. 2014, 2016) and to the study of flow-control techniques to reduce aero-optical distortions (Seidel et al. 2009). The use of POD in adaptive optics has greatly expanded as long time series of wave-front data became available from the Airborne Aero-Optics Laboratory (Jumper et al. 2013) and Airborne Aero-Optics Laboratory–Transonic programs (Jumper et al. 2015).

6. CONCLUDING REMARKS

The study of aero-optics is usually assumed to be an applied field, that is, useful only for providing information to assess or improve system performance for airborne free-space communication or directed energy systems. It is certainly that, and it is because this field of study is an enabling technology for these systems that funding has been available. Yet in this review, only Section 5 even mentioned these system-performance applications, as there has been much knowledge about fluid mechanics that has been learned from collecting and analyzing wave-front and wave-front-related data.

The analysis of aero-optical effects has already provided a good deal of information about flow characteristics and dynamics over a wide range of flow regimes for both Mach and Reynolds numbers. WFS and their derivative instruments now provide excellent spatial and temporal resolution and provide a nonintrusive method of interrogating a flow's density field as, at a minimum, a productive complementary experimental tool. Recent results make use of WFS to address the role of local pressure in boundary layers, analyze high-supersonic and hypersonic flows, and study transitional features in the flows described here. We believe these represent only the tip of the iceberg of things to come for applications of wave-front sensing methods to the study of fluid mechanics.

DISCLOSURE STATEMENT

The authors are not aware of any biases that might be perceived as affecting the objectivity of this review.

LITERATURE CITED

Abado S, Gordeyev S, Jumper EJ. 2010. Two-dimensional high-bandwidth Shack-Hartmann wavefront sensor: design guidelines and evaluation testing. *Opt. Eng.* 49:064403

Baskins LL, Hamilton LE. 1952. *Preliminary wind tunnel investigation on the optical transmission characteristics of a supersonic turbulent boundary layer*. Rep. G.M.-1.27, Northrop Aircr. Co., Hawthorne, CA

Baskins LL, Hamilton LE. 1954. *The effect of boundary layer thickness upon the optical transmission characteristics of a supersonic turbulent boundary layer*. Rep. NAI-54-756, Northrop Aircr. Co., Hawthorne, CA

Berkooz G, Holmes P, Lumley J. 1993. The proper orthogonal decomposition in the analysis of turbulent flows. *Annu. Rev. Fluid Mech.* 25:539–75

Born M, Wolf E. 1999. *Principles of Optics: Electromagnetic Theory of Propagation, Interference, and Diffraction of Light*. Cambridge, UK: Cambridge Univ. Press. 7th ed.

Burns R, Gordeyev S, Jumper EJ, Gogineni S, Paul M, et al. 2014. *Estimation of aero-optical wavefronts using optical and non-optical measurements*. Presented at AIAA Aerosp. Sci. Meet., 52th, National Harbor, MD, AIAA Pap. 2014-0319

Burns R, Jumper EJ, Gordeyev S. 2016. *A robust modification of a predictive adaptive-optic control method for aero-optics*. Presented at AIAA Plasmadyn. Lasers Conf., 47th, Washington, DC, AIAA Pap. 2016-3529

Cassady PE, Birch SF, Terry PJ. 1989. Aero-optical analysis of compressible flow over an open cavity. *AIAA J.* 27:758–62

Cicchiello JM, Jumper EJ. 1997. Far-field optical degradation due to near-field transmission through a turbulent heated jet. *Appl. Opt.* 36:6441–52

Cicchiello JM, Jumper EJ. 2001. *Low-order representation of fluid-optic interactions associated with a shear layer*. Presented at Aerosp. Sci. Meet., 39th, Reno, NV, AIAA Pap. 2001-0952

Cress J, Gordeyev S, Jumper EJ. 2010. *Aero-optical measurements in a heated, subsonic, turbulent boundary layer*. Presented at Aerosp. Sci. Meet., 48th, Orlando, FL, AIAA Pap. 2010-0434

De Lucca N, Gordeyev S, Jumper EJ. 2013. In-flight aero-optics of turrets. *Opt. Eng.* 52:071405

De Lucca N, Gordeyev S, Smith AE, Jumper EJ, Whiteley M, et al. 2014. *The removal of tunnel vibration induced corruption in aero-optical measurements*. Presented at AIAA Plasmadyn. Lasers Conf., 45th, Atlanta, GA, AIAA Pap. 2014-2494

Duan L, Beekman I, Martin MP. 2010. Direct numerical simulation of hypersonic turbulent boundary layers. Part 2. Effect of wall temperature. *J. Fluid Mech.* 655:419–45

Duffin DA. 2009. *Feed-forward adaptive-optic correction of a weakly-compressible high-subsonic shear layer*. PhD Thesis, Univ. Notre Dame

Duffner RW. 1997. *Airborne Laser: Bullets of Light*. New York: Basic

Faghihi A, Tesch J, Gibson S. 2013. Identified state-space prediction model for aero-optical wavefronts. *Opt. Eng.* 52:071419

Fitzgerald EJ, Jumper EJ. 2000. *Aperture effects on the aero-optical distortions measured for a compressible shear layer*. Presented at Aerosp. Sci. Meet., 38th, Reno, NV, AIAA Pap. 2000-0991

Fitzgerald EJ, Jumper EJ. 2002. Aperture effects on the aerooptical distortions produced by a compressible shear layer. *AIAA J.* 40:267–75

Fitzgerald EJ, Jumper EJ. 2004. The optical distortion mechanism in a nearly incompressible free shear layer. *J. Fluid Mech.* 512:153–89

Gao Q, Jiang Z, Yi S, Xie W, Liao T. 2012a. Correcting the aero-optical aberration of the supersonic mixing layer with adaptive optics: concept validation. *Appl. Opt.* 51:3922–29

Gao Q, Yi S, Jiang Z, He L, Wang X. 2012b. Optical transfer function of the supersonic mixing layer. *J. Opt. Soc. Am. A* 29:2628–37

Gaviglio J. 1987. Reynolds analogies and experimental study of heat transfer in the supersonic boundary layer. *Int. J. Heat Mass Transf.* 30:911–26

Gilbert KG. 1982. KC-135 aero-optical boundary-layer/shear-layer experiments. See Gilbert & Otten 1982, pp. 306–24

Gilbert KG. 2013. The challenge of high brightness laser systems: a photon odyssey. *Opt. Eng.* 52:071412

Gilbert KG, Otten LJ, eds. 1982. *Aero-Optical Phenomena*. Prog. Astronaut. Aeronaut. Vol. 80. New York: AIAA. 412 pp.

Gladstone JH, Dale TP. 1863. Researches on the refraction, dispersion, and sensitiveness of liquids. *Philos. Trans. R. Soc. Lond.* 153:317–43

Goodman JW. 1996. *Introduction to Fourier Optics*. New York: McGraw-Hill. 2nd ed.

Goorskey DJ, Drye R, Whiteley MR. 2013a. Dynamic modal analysis of transonic Airborne Aero-Optics laboratory conformal window flight-test aero-optics. *Opt. Eng.* 52:071414

Goorskey DJ, Schmidt J, Whiteley MR. 2013b. Efficacy of predictive wavefront control for compensating aero-optical distortions. *Opt. Eng.* 52:071418

Gordeyev S, Burns R, Jumper EJ, Gogineni S, Paul M, et al. 2013. *Aero-optical mitigation of shocks around turrets at transonic speeds using passive flow control*. Presented at AIAA Aerosp. Sci. Meet., 51st, Grapevine, TX, AIAA Pap. 2013-0717

Gordeyev S, Cress JA, Jumper EJ, Cain AB. 2011. Aero-optical environment around a cylindrical turret with a flat window. *AIAA J.* 49:308–15

Gordeyev S, Cress JA, Smith AE, Jumper EJ. 2015a. Aero-optical measurements in a subsonic, turbulent boundary layer with non-adiabatic walls. *Phys. Fluids* 27:045110

Gordeyev S, De Lucca N, Jumper EJ, Hird K, Juliano TJ, et al. 2014a. Comparison of unsteady pressure fields on turrets with different surface features using pressure sensitive paint. *Exp. Fluids* 55:1661

Gordeyev S, Hayden T, Jumper EJ. 2007a. Aero-optical and flow measurements over a flat-windowed turret. *AIAA J.* 45:347–57

Gordeyev S, Jumper EJ. 2010. Fluid dynamics and aero-optics of turrets. *Prog. Aerosp. Sci.* 46:388–400

Gordeyev S, Jumper EJ, Hayden T. 2012. Aero-optical effects of supersonic boundary layers. *AIAA J.* 50:682–90

Gordeyev S, Jumper EJ, Ng T, Cain A. 2003. *Aero-optical characteristics of compressible, subsonic turbulent boundary layer*. Presented at AIAA Plasmadyn. Lasers Conf., 34th, Orlando, FL, AIAA Pap. 2003-3606

Gordeyev S, Jumper EJ, Ng T, Cain A. 2005. *The optical environment of a cylindrical turret with a flat window and the impact of passive control devices*. Presented at AIAA Plasmadyn. Lasers Conf., 36th, Toronto, AIAA Pap. 2005-4657

Gordeyev S, Juliano TJ. 2016a. *Optical characterization of nozzle-wall Mach-6 boundary layers*. Presented at AIAA Aerosp. Sci. Meet., 54th, San Diego, CA, AIAA Pap. 2016-1586

Gordeyev S, Juliano TJ. 2016b. *Optical measurements of transitional events in a Mach-6 laminar boundary layer*. Presented at AIAA Fluid Dyn. Conf., 46th, Washington, DC, AIAA Pap. 2016-3348

Gordeyev S, Post M, MacLaughlin T, Ceniceros J, Jumper EJ. 2007b. Aero-optical environment around a conformal-window turret. *AIAA J.* 45:1514–24

Gordeyev S, Rennie RM, Cain AB, Hayden T. 2015b. *Aero-optical measurements of high-Mach supersonic boundary layers*. Presented at AIAA Plasmadyn. Lasers Conf., 46th, Dallas, TX, AIAA Pap. 2015-3246

Gordeyev S, Smith AE. 2016. *Studies of the large-scale structure in turbulent boundary layers using simultaneous velocity-wavefront measurements*. Presented at AIAA Plasmadyn. Lasers Conf., 47th, Washington, DC, AIAA Pap. 2016-3804

Gordeyev S, Smith AE, Cress JA, Jumper EJ. 2014b. Experimental studies of aero-optical properties of subsonic turbulent boundary layers. *J. Fluid Mech.* 740:214–53

Gordeyev S, Smith AE, Saxton-Fox T, McKeon B. 2015c. *Studies of the large-scale structure in adiabatic and moderately-wall-heated subsonic boundary layers*. Presented at TSFP-9, Melbourne, Pap. 7A-3

Greenwood BD, Primmerman CA. 1993. The history of adaptive-optics development and the MIT Lincoln Laboratory. *Proc. SPIE* 1920:220–34

Guarini SE, Moser RD, Shariff K, Wray A. 2000. Direct numerical simulations of a supersonic turbulent boundary layer at Mach 2.5. *J. Fluid Mech.* 414:1–33

Hardy JW. 1991. Adaptive optics: a progress review. *Proc. SPIE* 1542:2–17

Horwitz BA. 1993. Comparison approach for wavefront sensors. *Proc. SPIE* 1920:186–92

Houpt A, Gordeyev S, Juliano TJ, Leonov S. 2016. *Optical measurement of transient plasma impact on corner separation in* $M = 4.5$ *airflow*. Presented at AIAA Aerosp. Sci. Meet., 54th, San Diego, CA, AIAA Pap. 2016-2160

Hugo RJ, Jumper EJ. 1996. Experimental measurement of a time-varying optical path difference by the small-aperture beam technique. *Appl. Opt.* 35:4436–47

Hugo RJ, Jumper EJ. 2000. Applicability of the aero-optic linking equation to a highly coherent, transitional shear layer. *Appl. Opt.* 39:4392–401

Hugo RJ, Jumper EJ, Havener G, Stepanek SA. 1997. Time-resolved wavefront measurements through a compressible free shear layer. *AIAA J.* 35:671–77

Jumper EJ, ed. 2013. Special section on aero-optics and adaptive optics for aero-optics. *Opt. Eng.* 52(7, Spec. Issue). Bellingham, WA: SPIE

Jumper EJ, Gordeyev S, Cavalieri D, Rollins P, Whiteley MR, et al. 2015. *Airborne Aero-Optics Laboratory–Transonic (AAOL-T)*. Presented at AIAA Aerosp. Sci. Meet., 53rd, Kissimmee, FL, AIAA Pap. 2015-0675

Jumper EJ, Hugo RJ. 1995. Quantification of aero-optical phase distortion using the small-aperture beam technique. *AIAA J.* 33:2151–57
Jumper EJ, Fitzgerald EJ. 2001. Recent advances in aero-optics. *Prog. Aerosp. Sci.* 37:299–339
Jumper EJ, Zenk M, Gordeyev S, Cavalieri D, Whiteley MR. 2013. Airborne Aero-Optics Laboratory. *Opt. Eng.* 52:071408
Kamel M, Wang K, Wang M. 2016. *Predictions of aero-optical distortions using LES with wall modeling*. Presented at AIAA Aerosp. Sci. Meet., 54th, San Diego, CA, AIAA Pap. 2016-1462
Klein HH, Malley MM, Sapp O, Shough D, Sutton GW, et al. 1990. Experimental measurements of the optical path difference of a four-meter dual aerocurtain. *Proc. SPIE* 1221:404–13
Klein MV, Furtak TE. 1986. *Optics*. New York: Wiley. 2nd ed.
Kyrazis D. 2013. Airborne Laser Laboratory departure from Kirtland Air Force Base and a brief history of aero-optics. *Opt. Eng.* 52:071403
Lamberson S, Schall HB, Alvarado OL. 2005. *Overview of Airborne Laser's Test program*. Presented at US Air Force T&E Days Conf., Nashville, TN, AIAA Pap. 2005-7650
Liepmann HW. 1952. *Deflection and diffusion of a light ray passing through a boundary layer*. Tech. Rep. SM-14397, Douglas Aircr. Co., Santa Monica, CA
Maeder T, Adams NA, Kleiser L. 2001. Direct simulation of turbulent supersonic boundary layers by an extended temporal approach. *J. Fluid Mech.* 429:187–216
Mahajan VN. 1982. Strehl ratio for primary aberrations: some analytical results for circular and annular pupils. *J. Opt. Soc. Am.* 72:1258–66
Mahajan VN. 1983. Strehl ratio for primary aberrations in terms of their aberration variance. *J. Opt. Soc. Am.* 73:860–61
Malley M, Sutton GW, Kincheloe N. 1992. Beam-jitter measurements of turbulent aero-optical path differences. *Appl. Opt.* 31:4440–43
Masson B, Wissler J, McMackin L. 1994. *Aero-optical study of a NC-135 fuselage boundary layer.* Presented at Aerosp. Sci. Meet., 32nd, Reno, NV, AIAA Pap. 1994-0277
Mathews E, Wang K, Wang M, Jumper EJ. 2016. *LES of an aero-optical turret flow at high Reynolds number*. Presented at AIAA Aerosp. Sci. Meet., 54th, San Diego, CA, AIAA Pap. 2016-1461
McMackin L, Hugo RJ, Pierson RE, Truman CR. 1997. High speed optical tomography system for imaging dynamic transparent media. *Opt. Express* 1:302–11
McMackin L, Masson B, Clark N, Bishop K, Pierson R, et al. 1995. Hartmann wave front sensor studies of dynamic organized structure in flowfields. *AIAA J.* 33:2058–64
Moler JL, Lamberson S. 2013. The Airborne Laser (ABL): a legacy and a future for high-energy lasers. *Proc. SPIE* 3268:99–105
Morkovin MV. 1962. Effects of compressibility on turbulent flows. In *Mechanique de la Turbulence*, ed. A Favre, pp. 367–80. Paris: CNRS
Morrida J, Gordeyev S, De Lucca N, Jumper EJ. 2016a. Aero-optical investigation of shock-related effects on hemisphere-on-cylinder turrets at transonic speeds. *AIAA J.* In press
Morrida J, Gordeyev S, Jumper EJ. 2016b. *Transonic flow dynamics over a hemisphere in flight*. Presented at AIAA Aerosp. Sci. Meet., 54th, San Diego, CA, AIAA Pap. 2016-1349
Neal DR, O'Hern TJ, Torczynski JR, Warren ME, Shul R. 1993. Wavefront sensors for optical diagnostics in fluid mechanics: application to heated flow, turbulence and droplet evaporation. *Proc. SPIE* 2005:194–203
Nightingale AM, Gordeyev S, Jumper EJ. 2009. Optical characterization of a simulated weakly compressible shear layer: unforced and forced. *AIAA J.* 47:2298–305
Nightingale AM, Goodwine B, Lemmon M, Jumper EJ. 2013. Phase-locked-loop adaptive-optic controller and simulated shear layer correction. *AIAA J.* 51:2714–26
Nguyen M, Rennie RM, Gordeyev S, Jumper EJ, Cain AB, et al. 2015. *Wavefront measurements of a supersonic boundary layer using a laser-induced breakdown spark*. Presented at AIAA Plasmadyn. Lasers Conf., 46th, Dallas, TX, AIAA Pap. 2015-2804
Noll RJ. 1976. Zernike polynomials and atmospheric turbulence. *J. Opt. Soc. Am.* 66:207–11
Otten LG, Gilbert KG. 1982. Inviscid flowfield effects: experimental results. See Gilbert & Otten 1982, pp. 233–44

Pond J, Sutton G. 2006. Aero-optic performance of an aircraft forward-facing optical turret. *J. Aircr.* 43:600–7
Ponder ZB, Gordeyev S, Jumper EJ. 2011. *Passive mitigation of aero-induced mechanical jitter of flat-windowed turrets*. Presented at AIAA Plasmadyn. Lasers Conf., 42nd, Honolulu, HI, AIAA Pap. 2011-3281
Ponder ZB, Jumper EJ. 2011. *High-speed schlieren imaging through a two-dimensional weakly-compressible shear layer*. Presented at AIAA Aerosp. Sci. Meet., 49th, Orlando, FL, AIAA Pap. 2011-42
Ponder ZB, Rennie RM, Abado S, Jumper EJ. 2010. *Spanwise wavefront measurements through a two-dimensional weakly-compressible shear layer*. Presented at AIAA Plasmadyn. Lasers Conf., 41st, Chicago, IL, AIAA Pap. 2010-4495
Porter C, Gordeyev S, Jumper EJ. 2013a. Large-aperture approximation for not-so-large apertures. *Opt. Eng.* 52:071417
Porter C, Gordeyev S, Zenk M, Jumper EJ. 2013b. Flight measurements of the aero-optical environment around a flat-windowed turret. *AIAA J.* 51:1394–403
Porter C, Rennie M, Jumper EJ. 2013c. Aero-optic effects of a wingtip vortex. *AIAA J.* 51:1533–41
Ranade P, Duvvuri S, McKeon B, Gordeyev S, Christensen K, Jumper EJ. 2016. *Turbulence amplitude modulation in an externally-forced, subsonic turbulent boundary layer.* Presented at AIAA Aerosp. Sci. Meet., 54th, San Diego, CA, AIAA Pap. 2016-1120
Reid JZ, Lynch KP, Thurow BS. 2010. *Further development of a high-speed 3-D density measurement technique for aero-optics*. Presented at Fluid Dyn. Conf., 40th, Chicago, IL, AIAA Pap. 2010-4844
Reid JZ, Lynch KP, Thurow BS. 2013. Density measurements of a turbulent wake using acetone planar laser-induced fluorescence. *AIAA J.* 51:829–39
Rennie RM, Duffin DA, Jumper EJ. 2008. Characterization and aero-optic correction of a forced two-dimensional weakly compressible shear layer. *AIAA J.* 46:2787–95
Rose WC. 1979. *Measurements of aerodynamic parameters affecting optical performance*. Final Rep. AFWRL-TR-78-191, Air Force Weapons Lab., Kirtland Air Force Base, NM
Rose WC, Johnson DA, Otten LJ. 1982. Summary of ALL Cycle II.5 aerodynamic shear- and boundary-layer measurements. See Gilbert & Otten 1982, pp. 294–305
Rose WC, Otten LJ. 1982. Airborne measurement of atmospheric turbulence. See Gilbert & Otten 1982, pp. 325–40
Ross TS. 2009. Limitations and applicability of the Marechal approximation. *Appl. Opt.* 48:1812–18
Saxton-Fox T, Gordeyev S, Smith A, McKeon B. 2015. *Connections between density, wall-normal velocity, and coherent structure in a heated turbulent boundary layer.* Presented at Annu. Meet. APS Div. Fluid Dyn., 68th, Boston, MA
Saxton-Fox T, McKeon B, Smith A, Gordeyev S. 2014. *Simultaneous measurement of aero-optical distortion and turbulent structure in a heated boundary layer.* Presented at Annu. Meet. APS Div. Fluid Dyn., 67th, San Francisco, CA
Schmid PJ. 2010. Dynamic mode decomposition of numerical and experimental data. *J. Fluid Mech.* 656:5–28
Schwiegerling J, Neal DR. 2014. Historical development of the Shack-Hartmann wavefront sensor. *Proc. SPIE* 9186:91860U
Seidel J, Siegel S, McLaughlin T. 2009. *Computational investigation of aero-optical distortions in a free shear layer*. Presented at AIAA Aerosp. Sci. Meet., 47th, Orlando, FL, AIAA Pap. 2009-362
Siegel S, Seidel J, McLaughlin T. 2009. *Experimental study of aero-optical distortions in a free shear layer*. Presented at Aerosp. Sci. Meet., 47th, Orlando, FL, AIAA Pap. 2009-361
Siegenthaler J, Gordeyev S, Jumper E. 2005. *Shear layers and aperture effects for aero-optics.* Presented at AIAA Plasmadyn. Lasers Conf., 36th, Toronto, AIAA Pap. 2005-4772
Siegenthaler JP, Jumper EJ. 2007. Aperture effects in aero-optics and beam control. *J. Dir. Energy* 2(4):325–46
Small RD, Weihs D. 1976. Boundary layer effects in optical measurements in gas dynamics. *Appl. Opt.* 15:1591–94
Smith AE. 2015. *Evaluation of passive boundary layer flow control techniques for aero-optic mitigation*. PhD Thesis, Univ. Notre Dame
Smith AE, Gordeyev S, Ahmed H, Ahmed A, Wittich DJ, et al. 2014a. *Shack-Hartmann wavefront measurements of supersonic turbulent boundary layers in the TGF*. Presented at AIAA Plasmadyn. Lasers Conf., 45th, Atlanta, GA, AIAA Pap. 2014-2493

Smith AE, Gordeyev S, Jumper EJ. 2011. *Aero optics of subsonic boundary layers over backward steps*. Presented at AIAA Plasmadyn. Lasers Conf., 42nd, Honolulu, HI, AIAA Pap. 2011-3277

Smith AE, Gordeyev S, Saxton-Fox T, McKeon B. 2014b. *Subsonic boundary-layer wavefront spectra for a range of Reynolds numbers*. Presented at AIAA Plasmadyn. Lasers Conf., 45th, Atlanta, GA, AIAA Pap. 2014-2491

Smith DR, Smits AJ. 1993. Simultaneous measurement of velocity and temperature fluctuations in the boundary layer of supersonic flow. *Exp. Therm. Fluid Sci.* 7:221–29

Smits AJ, Dussauge JP. 1996. *Turbulent Shear Layers in Supersonic Flow*. Woodbury, NY: Am. Inst. Phys.

Speaker WV, Ailman CM. 1966. *Static and fluctuation pressures in regions of separated flow*. Presented at AIAA Aerosp. Sci. Meet., 4th, New York, AIAA Pap. 1966-456

Spina EF, Donovan JF, Smits AJ. 1991. Convection velocity in supersonic turbulent boundary layers. *Phys. Fluids A* 3:3124–26

Spina EF, Smits AJ, Robinson SK. 1994. The physics of supersonic turbulent boundary layers. *Annu. Rev. Fluid Mech.* 26:287–319

Steinmetz WJ. 1982. Second moments of optical degradation due to a thin turbulent layer. See Gilbert & Otten 1982, pp. 78–100

Stine HA, Winovich W. 1956. *Light diffusion through high-speed turbulent boundary layers*. Res. Memo. A56B21, Natl. Advis. Comm. Aeronaut., Washington, DC

Sutton GW. 1969. Effects of turbulent fluctuations in an optically active fluid medium. *AIAA J.* 7:1737–43

Sutton GW. 1985. Aero-optical foundations and applications. *AIAA J.* 23:1525–37

Tatarski VI. 1961. *Wave Propagation in a Turbulent Medium*. New York: McGraw-Hill

Thomas FO. 2015. *A new scaling for adverse pressure gradient turbulent boundary layers.* Presented at Euro. Turbul. Conf., 15th, Delft, The Netherlands

Trolinger JD. 1982. Aero-optical characterization of aircraft optical turrets by holography, interferometry and shadowgraph. See Gilbert & Otten 1982, pp. 200–17

Tromeur E, Garnier E, Sagaut P, Basdevant C. 2003. Large eddy simulations of aero-optical effects in a turbulent boundary layer. *J. Turbul.* 4:N5

Tyson RK. 1997. *Principles of Adaptive Optics*. New York: Academic. 2nd ed.

Visbal MR. 2009. *Numerical simulation of aero-optical aberration through weakly-compressible shear layers*. Presented at AIAA Fluid Dyn. Conf., 39th, San Antonio, TX, AIAA Pap. 2009-4298

Vorobiev A, Gordeyev S, Jumper EJ, Gogineni S, Marruffo A, et al. 2014. *Low-dimensional dynamics and modeling of shock-separation interaction over turrets at transonic speeds*. Presented at AIAA Plasmadyn. Lasers Conf., 45th, Atlanta, GA, AIAA Pap. 2014-2357

Vukasinovic B, Glezer A, Gordeyev S, Jumper EJ, Kibens V. 2008. *Active control and optical diagnostics of the flow over a hemispherical turret*. Presented at Aerosp. Sci. Meet., 46th, Reno, NV, AIAA Pap. 2008-0598

Vukasinovic B, Glezer A, Gordeyev S, Jumper EJ, Kibens V. 2011. Hybrid control of a turret wake. *AIAA J.* 49:1240–55

Wang K, Wang M. 2009. *Numerical simulation of aero-optical distortions by a turbulent boundary layer and separated shear layer*. Presented at AIAA Plasmadyn. Lasers Conf., 40th, San Antonio, TX, AIAA Pap. 2009-4223

Wang K, Wang M. 2013. On the accuracy of Malley probe measurements of aero-optical effects: a numerical investigation. *Opt. Eng.* 52:071407

Wang K, Wang M, Gordeyev S, Jumper EJ. 2010. *Computation of aero-optical distortions over a cylindrical turret with passive flow control.* Presented at AIAA Plasmadyn. Lasers Conf., 41st, Chicago, IL, AIAA Pap. 2010-4498

Wang M, Mani A, Gordeyev S. 2012. Physics and computation of aero-optics. *Annu. Rev. Fluid Mech.* 44:299–321

Weston CP, Jumper EJ. 2002. *Influence of periodic compressible vortices on laser beam intensity.* Presented at AIAA Plasmadyn. Lasers Conf., 33rd, Maui, AIAA Pap. 2002-2276

Wittich DJ. 2009. *Subsonic flow over open and partially-covered, rectangular cavities*. PhD Thesis, Univ. Notre Dame

Wittich DJ, Gordeyev S, Jumper EJ. 2007. *Revised scaling of optical distortions caused by compressible, subsonic turbulent boundary layers.* Presented at AIAA Plasmadyn. Lasers Conf., 38th, Miami, FL, AIAA Pap. 2007-4009

Wittich DJ, Paul M, Ahmed H, Ahmed A, Smith AE, et al. 2014. *Aero-optic characterization of supersonic boundary layers in the Trisonic Gasdynamic Facility*. Presented at AIAA Plasmadyn. Lasers Conf., 45th, Atlanta, GA, AIAA Pap. 2014-2356

White MD, Visbal MR. 2012. *Aero-optics of compressible boundary layers in the transonic regime*. Presented at AIAA Plasmadyn. Lasers Conf., 43rd, New Orleans, LA, AIAA Pap. 2012-2984

White MD, Visbal MR. 2013. *Computational investigation of wall cooling and suction on the aberrating structures in a transonic boundary layer*. Presented at AIAA Aerosp. Sci. Meet., 51st, Grapevine, TX, AIAA Pap. 2013-0720

Whiteley MR, Goorskey DJ, Drye R. 2013. Aero-optical jitter estimation using higher-order wavefronts. *Opt. Eng.* 52:071411

Wolters DJ. 1973. *Aerodynamic effects on airborne optical systems*. Tech. Rep. MDC A2582, McDonnell Douglas Corp., St. Louis, MO

Wyckham CM, Smits AJ. 2009. Aero-optic distortion in transonic and hypersonic turbulent boundary layers. *AIAA J.* 47:2158–68

Zubair FR, Catrakis HJ. 2007. Aero-optical interactions along laser beam propagation paths in compressible turbulence. *AIAA J.* 45:1663–74

Annual Review of
Fluid Mechanics

Volume 49, 2017

Contents

Indexes

Errata

An online log of corrections to *Annual Review of Fluid Mechanics* articles may be found at http://www.annualreviews.org/errata/fluid